The Structural Characterization of Oligonucleotide-Modified Gold Nanoparticle Networks Formed by DNA Hybridization

So-Jung Park,[†] Anne A. Lazarides,[†,‡] James J. Storhoff, Lorenzo Pesce, and Chad A. Mirkin*

Department of Chemistry and Institute for Nanotechnology, Northwestern University, Evanston, Illinois 60208

Received: March 23, 2004

The structural properties of DNA-linked gold nanoparticle materials were examined using synchrotron small-angle X-ray scattering. The materials are composed of 12 or 19 nm diameter gold particles modified with 3′ or 5′ alkylthiol-capped 12-base oligonucleotides and linked with complementary oligonucleotides. Structure factors were derived from scattering intensities, and nearest-neighbor distances were determined from the primary peak in the pair distance distribution functions. The separation between particles was found to increase linearly with DNA linker length for 24, 48, and 72 base pair linkers. For assemblies formed in 0.3 M NaCl, 10 mM phosphate buffer solution, the increment in the interparticle distance was found to be 2.5 Å per base pair. Particle separations in assemblies at lower electrolyte concentration were larger, indicating that dielectric screening modulates the interactions. The effect of DNA sequence was studied with poly-adenine or poly-thymine spacer sequences incorporated between the alkylthiol and recognition sequences. The assemblies with poly-adenine spacer sequences showed significantly shorter particle separations than the assemblies involving poly-thymine spacers, a consequence of their different affinities for the gold surface. While the scattering data do not display evidence of long-range order, pair distance distribution functions indicate the presence of short-range order.

Introduction

Recently, there has been considerable effort aimed at developing strategies for assembling nanoparticles into two- and three-dimensional functional structures.[1] Because such structures exhibit collective physical and chemical properties that are dependent upon their architectural parameters,[1−8] the ability to deliberately organize nanoparticles into a preconceived structure is essential for achieving maximum control over desired properties. A variety of assembly schemes have been developed based upon DNA, proteins, small organic molecules, and synthetic polymers as particle linkers, and, thus far, insulators, semiconductors, and metallic nanoparticles as well as multivalent proteins have been used as particle building blocks.[9−16]

DNA has been demonstrated to be a particularly versatile construction material due to its flexible length scale and rigid and chemically programmable duplex structure.[17] Over the past few years, researchers have demonstrated that one can use DNA to control the assembly of nanoparticles in solution in the form of aggregates (Scheme 1A) and small clusters (Scheme 1B) and off of surfaces in the form of multilayered structures (Scheme 1C).[9,13,18−20] These materials have been used to develop a variety of biomolecule detection schemes based upon their collective optical, catalytic, or electrical properties.[21−25] The most extensively studied and characterized DNA-driven nanoparticle linking system is the three DNA strand system, Scheme 1A,[9] applied to gold nanoparticles. In this system, two sets of oligonucleotide-modified nanoparticles are connected by complementary linking DNA to form extended structures. Those

SCHEME 1

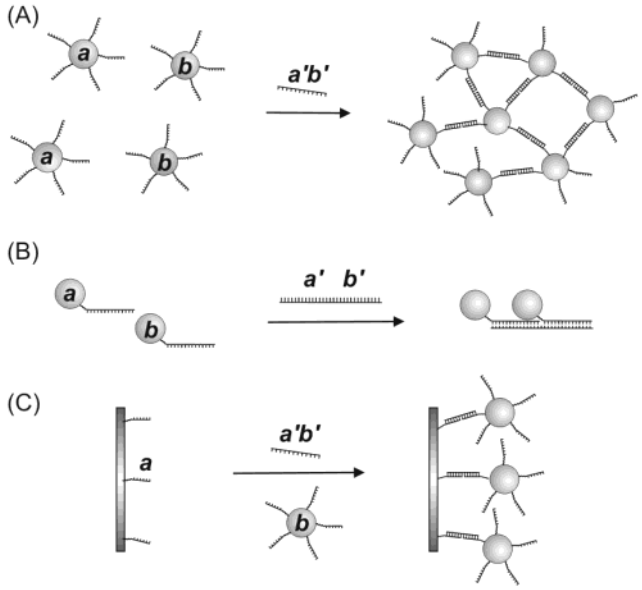

structures have been characterized by transmission electron microscopy (TEM),[9,26] dynamic light scattering (DLS),[26] and ultrasmall-angle X-ray scattering experiments (USAXS).[27] While TEM only provides two-dimensional information on sedimented, desiccated assemblies and DLS and USAXS provide only ensemble-averaged data, collectively they provide both direct imaging and in situ, aqueous phase evidence of extended assembly formation. From the USAXS data, the assemblies are understood to be space-filling as opposed to fractal. Herein, we describe a detailed study of the aqueous phase, three-dimensional structure of a variety of DNA-linked nanoparticle assemblies. To investigate interparticle structure, we use synchrotron small-

* To whom correspondence should be addressed. E-mail: camirkin@chem.northwestern.edu.

† These authors contributed equally to this work.

‡ Present address: Department of Mechanical Engineering and Materials Science, Duke University, Durham, NC 27708.

10.1021/jp040242b CCC: $27.50
Published on Web 07/27/2004

SCHEME 2

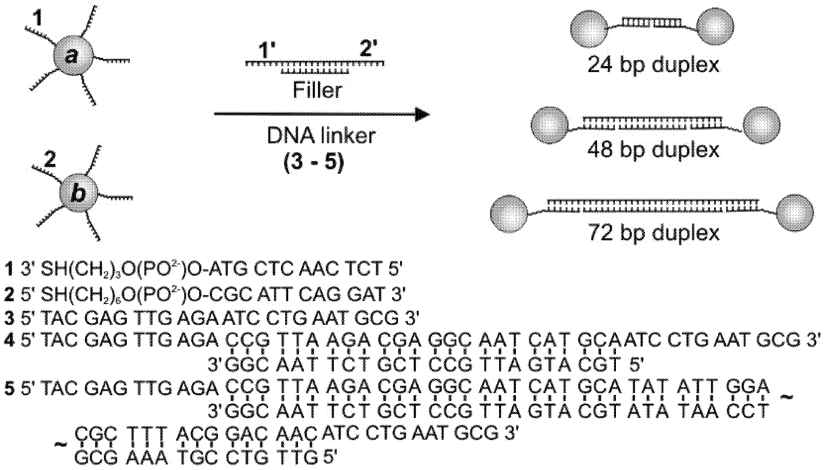

angle X-ray scattering (SAXS) in a q-range that provides information on structure in the few to tens of nanometer length scale. The following issues have been addressed. First, how do interparticle spacings vary with number of bases in the DNA interconnect and size of the nanoparticle building blocks? Second, how do interparticle interactions and DNA−nanoparticle interactions affect the resulting three-dimensional structure? To provide a basis for comparison, we have considered systems (Scheme 2) that have been extensively characterized by UV−vis spectroscopy, conductivity measurements, melting analyses, transmission electron microscopy, and light-scattering experiments.[26,28] Some prior results on the interparticle spacing control provided by duplex DNA have been presented in refs 11, 26, and 28.

Experimental Section

Preparation of Oligonucleotide-Modified Gold Nanoparticles and Linker DNA. The synthesis of alkylthiol-capped oligonucleotides (**1**, **2**) and the immobilization of them on gold nanoparticles were described elsewhere.[22] Linker DNA strands (**3**−**5**) were synthesized and purified via literature methods.[22] Gold particles of ∼12 nm diameter were prepared by citrate reduction of $HAuCl_4$.[29] Gold particles of ∼19 nm diameter were purchased from Ted Pella. The oligonucleotide-modified gold nanoparticles were indefinitely stable (over a year) to agglomeration in salt solution (0.3 M NaCl) as evidenced by no change in the UV−vis spectroscopy of the aqueous suspension of particles. The solutions containing oligonucleotide-modified nanoparticles were filtered through an acetate syringe filter (0.22 μm) prior to SAXS experiments. Longer duplex linkers (48- and 72-mer) were prepared by hybridizing 48- and 72-mer single-stranded oligonucleotides with 24- and 48-mer filler DNA, respectively, Scheme 2.

Preparation of Nanoparticle Assemblies. To form nanoparticle networks, equal amounts of oligonucleotide-modified nanoparticles, **a** and **b** (10 nM, 130 μL) were combined in a microcentrifuge tube, and linker DNA, **3**−**5** (10 μM, 6 μL), was added to the nanoparticle mixture. Except for the experiments aimed at probing the effect of particle size on aggregate structure, 12 nm particles were used for all other experiments. Unless otherwise mentioned, nanoparticle aggregates were formed in 0.3 M NaCl, 10 mM phosphate buffer at pH 7 (PBS) and were annealed at 45 °C for 15 min.

SAXS Measurements. The SAXS experiments were performed at the Dupont-Northwestern-Dow Collaborative Access Team (DND-CAT) Sector 5 of the Advanced Photon Source, Argonne National Laboratory with X-rays of wavelength 1.54 Å (8 keV) or 1.24 Å (10 keV). Aqueous samples were placed in 0.8 or 1.2 mm flat cells between Kapton windows. Two sets of slits were used to define and collimate the X-ray beam, and a pinhole was used to remove parasitic scattering. Samples were irradiated with a 0.3 × 0.3 mm^2 beam, and scattered radiation was detected with a CCD area detector. The 2D scattering data were azimuthally averaged, and the resulting 1D profiles of scattered intensity as a function of scattering angle, 2θ, were transformed into profiles of scattered intensity as a function of scattering vector, s ($=2\sin(\theta)/\lambda$), using silver behenate[30] as a standard. All data were corrected for background scattering and sample absorption. In this system, scattering from DNA is negligible as compared to that from electron dense gold; scattering from the buffer and windows is weak relative to that from the gold, but the buffer data are nonetheless used to reduce the solution sample data to scattering representative of the particles alone.

Results and Discussion

Scattering from Dispersed DNA-Modified Nanoparticles. SAXS data were collected from mixtures of dispersed DNA-modified nanoparticles, Figure 1. The scattering patterns display fringes characteristic of dispersions of noninteracting particles with modest dispersity in size and shape.[31,32] Particle sizing was accomplished by fitting the profiles with ensemble-averaged differential scattering cross sections, that is, profiles evaluated using the expression $I(s) = I_e \int P(\xi) N_e^2(\xi) F^2(s;\xi)\, d\xi$ where I_e is the "constant" differential scattering cross section for a single electron in the forward direction; P is the probability density for the shape and size distribution; N_e ($=Vn_e$) is the electron number equal to the particle volume, V, times the excess electron density, n_e, of the nanoparticles relative to the solvent; and $F^2(s;\xi)$ is the form factor of a single particle with shape and size indexed by ξ.[31] Initially, the profiles were calculated assuming spherical particles with Gaussian distributions of radii, r, for which the square root, F, of the form factor is proportional to the spherical Bessel function, $j_1(x) = (\sin(x) - x\cos(x))/x^3$, where $x = 2\pi sr$. These fits were compared to fits obtained from ensembles of spheroidal particles with distributions in aspect ratio as well as size.

Figure 1A shows an experimental profile for the 12 nm particles that is composed of short exposure (10 s) data at low angle and longer exposure (240 s) data at high angle.[33] An ensemble-averaged calculated profile is shown as well. The ensemble was modeled as a population of spheroidal particles

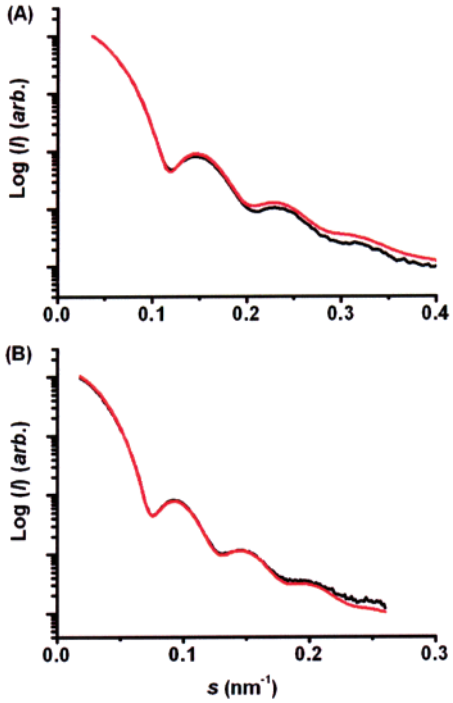

Figure 1. Scattering patterns from dispersed particles (black) and ensemble-averaged calculated profiles (red) for (A) 12.0 ± 1 nm particles and (B) 19 ± 1.2 nm particles.

with Gaussian distributions in size and aspect ratio. Fitting yielded a size distribution of 12.0 ± 1.0 nm and an aspect ratio distribution of 1.0 ± 0.1. Alternatively, an assumption of particle sphericity yielded a size distribution of 11.8 ± 1.2 nm. Figure 1B shows the experimental profile for the 19 nm particles along with an ensemble-averaged calculated profile. The ensemble was modeled as a population of spheroidal particles with an aspect ratio of 1.0 ± 0.2 and size of 19.0 ± 1.2 nm. The alternative fit assuming no eccentricity yielded a size distribution of 18.8 ± 1.9 nm.

Nanoparticle Aggregates Formed from Different Length DNA Interconnects and Different Sized Nanoparticles. The oligonucleotide-modified nanoparticles (**a**, **b**) were assembled into extended networks using three different DNA interconnects, 24-mer, 48-mer, and 72-mer strands, Scheme 2. Note that the 24-mer linker is a single-stranded oligonucleotide and the 48- and 72-mer linkers are duplex DNA with "sticky" ends that are complementary to the oligonucleotides on the nanoparticles. Upon aggregate formation, the red nanoparticle solution turned purple, and the nanoparticle aggregates precipitated from solution. The small-angle scattering patterns of the DNA-linked nanoparticle assemblies display interference peaks in addition to the fringe patterns of the dispersed particles. Given the monodispersity of the particles, the structure factor, S, of the nanoparticle assemblies can be determined by dividing the scattered intensity, I_{agg}, by the intensity from the noninteracting particle dispersions, I_{disp} (Figure 1), after correcting for buffer, window, and parasitic scattering, as described in eq 1.[32,34]

$$I_{agg}(\theta) \propto I_{disp}(\theta)S(\theta) \qquad (1)$$

The diffraction peaks are well defined, and they shift to smaller angles with increasing base pair number in the DNA linkers, indicating larger interparticle spacing, Figure 2.

To examine the role of DNA duplex structure in defining assembly structure, nanoparticle aggregates were prepared using single-stranded 72-mer linker without the complementary 48-

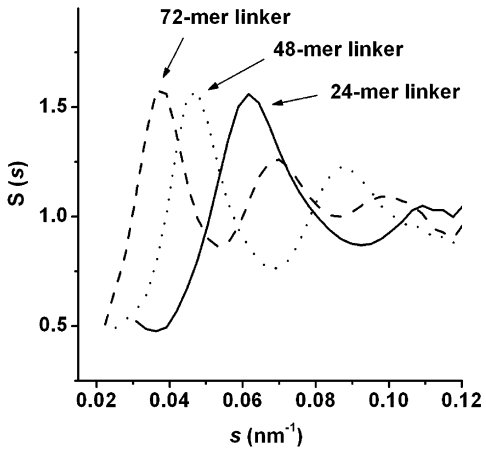

Figure 2. The structure factors of nanoparticle aggregates formed from 12 nm particles and three different linkers, 24-mer, 48-mer, and 72-mer, in 0.3 M PBS solutions.

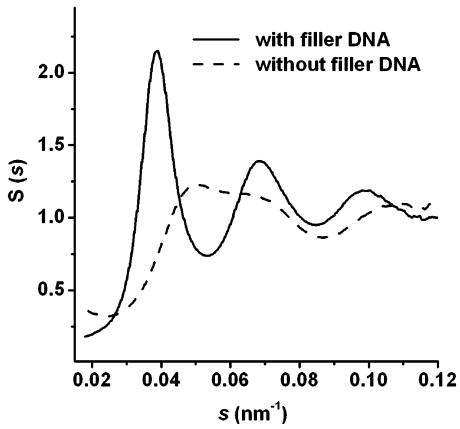

Figure 3. The structure factors of nanoparticle aggregates formed from 72-mer duplex linkers (solid line) and nanoparticle aggregates formed from single-stranded 72-mer oligonucleotides without filler DNA (dashed line). Both samples were prepared from 12 nm particles in 0.3 M PBS solutions.

base "filler" strand. As compared to the aggregates formed from duplex linkers, the aggregates formed using single-stranded DNA linkers show a significantly less well-defined scattering pattern, Figure 3. This result indicates that the rigid nature of DNA duplex is critical for the formation of a well-defined assembly structure in which DNA base pair number controls the interparticle spacing.

To obtain interparticle distances within the assemblies, the pair distance distribution functions (PDDF), $g(r)$,[32] were calculated from the structure factors, $S(s)$, using eq 2, where ρ is the particle number density, Figure 4.

$$g(r) = 1 + 2\rho r \int s(S(s) - 1)\sin(2\pi sr)\,ds \qquad (2)$$

The PDDF gives the probability of finding a second particle at a given distance, r, from a given particle; thus, the low-r peak position of each PDDF corresponds to the nearest-neighbor center-to-center distance, D_{nn}, for that assembly. When D_{nn} values for various assemblies are plotted as a function of linker base pair number, they display a linear relationship, Figure 5.

In addition to the 12 nm particles, 19 nm particles were used to form the same types of assemblies and examined by SAXS. Interparticle spacings as given by the PDDFs for the larger particle assemblies also display a linear relationship with base pair number, with offsets of ~7 nm from the spacings found in

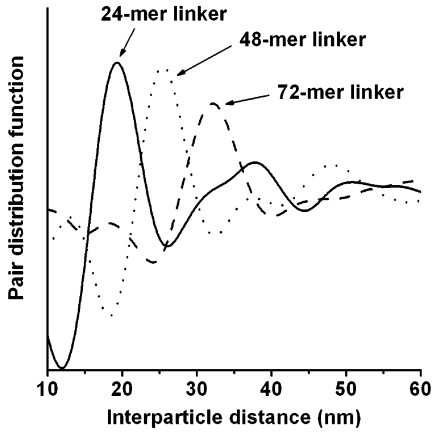

Figure 4. PDDFs of the scattering patterns from nanoparticle aggregates linked by three different length DNA linkers presented in Figure 2. The primary peak positions of the PDDFs indicate the nearest-neighbor distances.

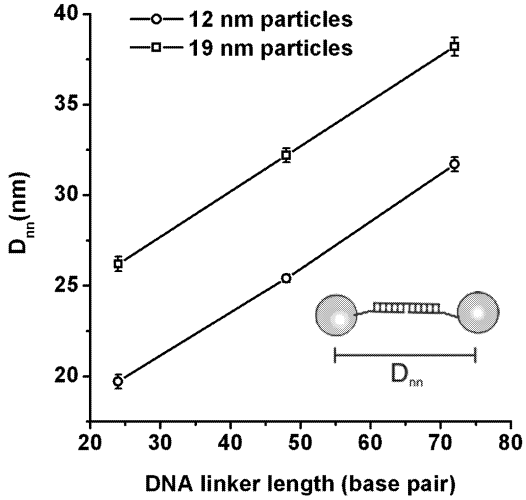

Figure 5. Center-to-center interparticle distances obtained from PDDFs as a function of linker length. Nanoparticle aggregates were formed from two different sized particles, 12 and 19 nm particles in 0.3 M PBS solutions. The particle separation increases linearly with DNA linker length for both cases.

assemblies of 12 nm particles, Figure 5. Note that the offset of 7 nm matches the particle size difference. From the slopes of the plots, the increase of D_{nn} per one base pair is found to be 0.25 nm, which is shorter than the length per base pair of B-form DNA, 0.34 nm.[35] Possible explanations are that (1) interparticle spaces are determined by multiple DNA duplex linkers that connect regions of the particle surface offset from the point of closest approach, or (2) particle-linked DNA has a different conformation than solution-phase B form DNA. The latter possibility is not unreasonable given the high dielectric environment and the possibly condensed nature of the oligonucleotide environment. Nonetheless, the results demonstrate that particle spacings in DNA-linked nanoparticle assemblies can be tailored by using different DNA duplex interconnects.

For comparison, 24-mer-linked nanoparticle aggregates were formed by a two-strand system in addition to the three-strand system described thus far. In the two-strand system, the aggregates were formed by mixing two sets of nanoparticles modified with complementary 24-mer oligonucleotides. The assemblies formed by the two different methods but with the same linker length showed scattering peaks at approximately the same positions. The effects of particle and linker concentrations and of annealing also were investigated; no significant effect on the interparticle distances was observed.

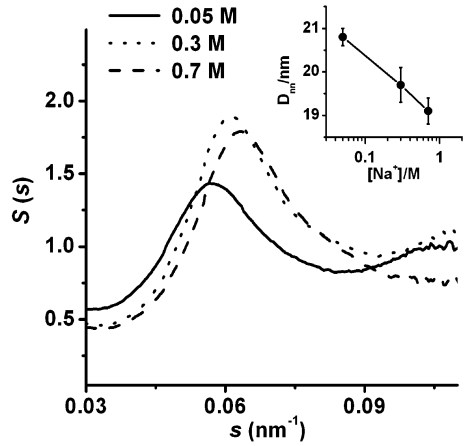

Figure 6. The structural factors of 24-mer-linked 12 nm particle aggregates formed in buffer solutions of different salt concentration. Inset: Interparticle distances as a function of NaCl concentration.

Particle Packing within DNA-Linked Nanoparticle Assemblies. Typically, monodisperse hard spheres crystallize into closely packed structures. Metal particles, however, interact through long-range attractive forces as well as hard repulsive forces, and charge or sterically stabilized particles interact through a complex interplay of distance-dependent attractive and repulsive interactions. Thus, depending on the types of particles and ligand molecules and the preparation conditions, chemically functionalized particles assemble into a variety of morphologies and may display a rich phase behavior.[36,37] Oligonucleotide-modified nanoparticles provide a unique system to study superstructure formation in the presence of both repulsive and attractive interactions.[37]

DNA-linked nanoparticle assemblies have scattering patterns analogous to those of amorphous materials, that is, materials that display short-range, though not long-range order. A comparison of nearest-neighbor distances, revealed by the PDDFs, and the *d* spacings determined by peaks in the structure factors confirms the presence of short-range order. Specifically, for all linked assemblies, the scattering patterns display (1) an absence of a peak at the angle corresponding to the *d* spacing, D_{nn}, for the nearest-neighbor distance as determined by the PDDF and (2) a maximally intense, lowest angle peak at an angle corresponding to a *d* spacing of $(\sqrt{2}/\sqrt{3})D_{nn}$. This behavior is characteristic of systems whose "atomic" bases null intensity in the scattering direction corresponding to nearest-neighbor planes such as body-centered cubic (BCC), face-centered cubic (FCC), or closely related body-centered tetragonal (BCT) structures. While these structural properties are shared by all linked assemblies considered here, that is, assemblies with particle size to linker lengths in the range of 0.4−2.0 particle radii, it is by no means universal among DNA-linked particle assemblies. Rather, other linking systems have been observed to result in alternative structures. For example, assemblies composed of structurally incommensurate component "particles", such as the protein/nanoparticle system described in ref 11, have scattering patterns that are quantitatively different. Nonetheless, the extensive interference displayed in the scattering data for all of the DNA-linked nanoparticle systems that we have studied indicates local order and an absence of the fractal structure observed in aggregates of bare particles.[38]

The Effect of Ionic Strength. In the absence of complementary linking DNA, the oligonucleotide-modified nanopar-

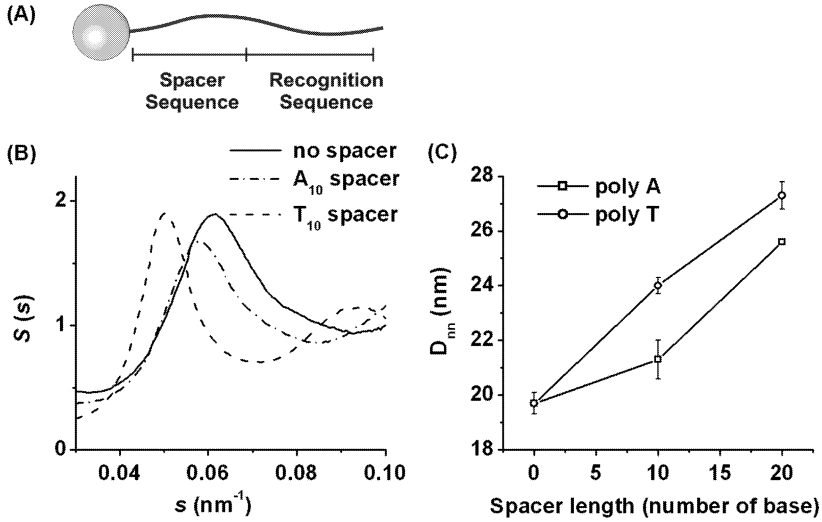

Figure 7. (A) A drawing describing the spacer DNA. (B) The structure factors of 24-mer-linked aggregates formed from 12 nm particles with A_{10} (sequence: AAA AAA AAA A), T_{10} (sequence: TTT TTT TTT T), or no spacer sequence. (C) The interparticle distances as a function of spacer DNA length for poly-A and poly-T spacers. The two systems show distinct signatures due to their different binding strength to gold surface. For all samples, aggregates were prepared in 0.3 M PBS solutions.

ticles are uniformly dispersed in a buffer solution due to the repulsive interaction between like-charged nanoparticles. In DNA-linked assemblies, electrostatic forces are nonetheless expected to play a significant role in mediating the attractive interactions between complementary DNA strands and may also affect the assembly superstructure.[39] To examine this effect, nanoparticle aggregates were formed in a series of buffer solutions with different ionic strengths. As the salt concentration of the buffer is lowered, the diffraction peaks shift to lower angles, indicating larger interparticle spacings, Figure 6. When NaCl concentration is varied over the range of 0.05−0.7 M, the spacing between 24-mer-linked particles changes by ∼1.7 nm, Figure 6, inset. At high salt concentration, cations screen the negative charge of the oligonucleotides on the nanoparticles, allowing particles to assemble more closely, while, at low salt concentration, particle−particle repulsion becomes stronger and results in larger interparticle spacings.

The Effect of Single-Strand Spacer DNA. In the design of oligonucleotide sequences, we have employed spacer sequences in addition to the recognition strands, Figure 7A. Interestingly, the type and length of spacer DNA affect the properties of the oligonucleotide-modified nanoparticles, such as their hybridization efficiencies and the thermal denaturation temperatures of the resulting duplex structures.[40] From a study of nucleoside binding on gold nanoparticles and on planar surfaces,[41,42] we have postulated that this effect is due to the different affinity of the four DNA bases to the gold surfaces. We expect that differences in binding affinities of different oligonucleotide sequences should manifest themselves both as differences in spacer configuration and also as differences in aggregate superstructure. Here, we seek to demonstrate that the information of interest can be derived from scattering studies of DNA-linked nanoparticles.

For this purpose, nanoparticles were modified with oligonucleotides with poly-adenine or poly-thymine spacers incorporated between the surface-binding alkylthiol and the recognition sequence, Figure 7A. Subsequently, the nanoparticles were assembled using 24-mer linkers. Interestingly, the assemblies involving A_{10} and T_{10} spacer units showed scattering peaks at quite different angles, despite their identical base number, Figure 7B. When the particles with an A_{10} spacer were linked by 24-mer DNA, interparticle spacing increased by only about 1.6 nm, as compared to the spacer-free system, while the insertion of a T_{10} spacer increased the interparticle spacing by approximately 4.3 nm. These results clearly indicate that ssDNA composed of poly-adenine has a high affinity for gold which is manifested by a tendency to lie on the surface, while poly-thymine has a low affinity and tends to stand upright and away from the surface.[43] This is consistent with previous spectroscopic studies aimed at determining such interactions.[41,42,44]

Because the interactions between single-stranded oligonucleotides and a gold surface are complex and possibly surface area limited, the number of bases in the single-stranded spacer DNA and the interparticle distances do not display a simple linear relationship, such as that seen when varying base pair number in the duplex portion of the linker, Figure 7C. In addition, assemblies involving different types of spacer sequences show distinct signatures due to the difference in their binding strength. In the case of poly-A, a major portion of the A_{10} spacer is coordinated to the particle surface due to its high affinity to gold. As the number of spacer bases increases, a portion will bind on the surface and the rest will stand out, as evidenced by the significant increase in interparticle spacing with longer poly-A spacer, A_{20}, as compared to the system with an A_{10} spacer. In the case of poly-T, because it has a low affinity for gold, the interparticle spacing gradually increases with increasing spacer length.

Conclusions

We have studied a number of factors that control the structural parameters of DNA-linked nanoparticle assemblies. When oligonucleotide-modified nanoparticles are connected by duplex DNA linkers, the assemblies exhibit relatively sharp scattering peaks. While the assemblies are not crystalline, the scattering patterns and derived PDDFs together reveal that the assemblies have FCC-, BCC-, or BCT-like local structure.

Importantly, the assemblies formed from different length oligonucleotide linkers (24-, 48-, and 72-mer) show an increase in particle spacing as the base pair number of the linker DNA is increased. This result demonstrates that we can indeed take advantage of the flexible length scale and the rigid duplex structure of DNA to tailor interparticle spacings using different length DNA interconnects.

Small-angle X-ray scattering has also been used to probe the effects of surface interaction on the assembly structure. Oligonucleotides composed of poly-A have high affinities for gold, and incorporation of a poly-A spacer unit increases the interparticle spacing by only a small amount. In contrast, poly-T has a relatively low affinity for gold, and a poly-T spacer significantly increases the interparticle spacing. This study demonstrates the importance of DNA/nanoparticle interactions in DNA-based assembly schemes. Even if the nanoparticles are modified with oligonucleotides of equal base number, assemblies with different structures can result depending on the choice of spacer DNA sequences.

Because many interesting properties of nanoparticle-based materials are highly dependent upon their structural parameters, it is important to understand how assembly structure depends on the various building blocks, interconnects, and assembly conditions. The study described herein was designed to explore these relationships in DNA-linked assemblies and thereby provide insight into the structural basis for some of the important physical properties associated with these assemblies. Ultimately, an understanding of the mechanisms of structural control in hybrid systems of this type will enable the design of the materials with targeted properties.

Acknowledgment. C.A.M. acknowledges DARPA, AFOSR, and NSF. A.A.L. acknowledges the support of G. C. Schatz and the ARO. The SAXS experiments were performed with the support of the Dupont Northwestern Dow Collaborative Access Team (DND-CAT) at Sector 5 of the Advanced Photon Source. Preliminary experiments were performed with the support of the Biological SAXS/Diffraction staff of BL 4-2 at the Stanford Synchrotron Radiation Laboratory.

References and Notes

(1) Storhoff, J. J.; Mucic, R. C.; Mirkin, C. A. *J. Cluster Sci.* **1997**, *8*, 179.
(2) Fendler, J. H.; Meldrum, F. C. *Adv. Mater.* **1995**, *7*, 607.
(3) Bethell, D.; Brust, M.; Schiffrin, D. J.; Kiely, C. *J. Electroanal. Chem.* **1996**, *409*, 137.
(4) Bethell, D.; Schiffrin, D. J. *Nature* **1996**, *382*, 581.
(5) Weller, H. *Angew. Chem., Int. Ed. Engl.* **1996**, *35*, 1079.
(6) Alivisatos, A. P. *Science* **1996**, *271*, 933.
(7) Heath, J. R. *Science* **1995**, *270*, 1315.
(8) Schmid, G.; Chi, L. F. *Adv. Mater.* **1998**, *10*, 515.
(9) Mirkin, C. A.; Letsinger, R. L.; Mucic, R. C.; Storhoff, J. J. *Nature* **1996**, *382*, 607.
(10) Mitchell, G. P.; Mirkin, C. A.; Letsinger, R. L. *J. Am. Chem. Soc.* **1999**, *121*, 8122.
(11) Park, S.-J.; Lazarides, A. A.; Mirkin, C. A.; Letsinger, R. L. *Angew. Chem., Int. Ed.* **2001**, *40*, 2909.
(12) Cao, Y. W.; Jin, R.; Mirkin, C. A. *J. Am. Chem. Soc.* **2001**, *123*, 7961.
(13) Alivisatos, A. P.; Johnsson, K. P.; Peng, X.; Wilson, T. E.; Loweth, C. J.; Bruchez, M. P., Jr.; Schultz, P. G. *Nature* **1996**, *382*, 609.
(14) Shenton, W.; Davis, S. A.; Mann, S. *Adv. Mater.* **1999**, *11*, 449.
(15) Connolly, S.; Fitzmaurice, D. *Adv. Mater.* **1999**, *11*, 1202.
(16) Brust, M.; Bethell, D.; Kiely, C. J.; Schiffrin, D. J. *Langmuir* **1998**, *14*, 5425.
(17) Storhoff, J. J.; Mirkin, C. A. *Chem. Rev.* **1999**, *99*, 1849.
(18) Taton, T. A.; Mucic, R. C.; Mirkin, C. A.; Letsinger, R. L. *J. Am. Chem. Soc.* **2000**, *112*, 6305.
(19) Niemeyer, C. M.; Burger, W.; Peplies, J. *Angew. Chem., Int. Ed.* **1998**, *37*, 2265.
(20) Soto, C. M.; Srinivasan, A.; Ratna, B. R. *J. Am. Chem. Soc.* **2002**, *124*, 8508.
(21) Elghanian, R.; Storhoff, J. J.; Mucic, R. C.; Letsinger, R. L.; Mirkin, C. A. *Science* **1997**, *277*, 1078.
(22) Storhoff, J. J.; Elghanian, R.; Mucic, R. C.; Mirkin, C. A.; Letsinger, R. L. *J. Am. Chem. Soc.* **1998**, *120*, 1959.
(23) Park, S.-J.; Taton, T. A.; Mirkin, C. A. *Science* **2002**, *295*, 1503.
(24) Taton, T. A.; Mirkin, C. A.; Letsinger, R. L. *Science* **2000**, *289*, 1757.
(25) Cao, Y. W. C.; Jin, R. C.; Mirkin, C. A. *Science* **2002**, *297*, 1536.
(26) Storhoff, J. J.; Lazarides, A. A.; Mirkin, C. A.; Letsinger, R. L.; Mucic, R. C.; Schatz, G. C. *J. Am. Chem. Soc.* **2000**, *122*, 4640.
(27) Lazarides, A. A. (unpublished results). USAXS experiments on 24 base pair-linked 12 nm Au particle assemblies not only indicated the presence of large assemblies, but also yielded a fractal dimension for these assemblies of 2.8 ± 0.2. From this we conclude that the assemblies are essentially space-filling, that is, not fractal.
(28) Park, S.-J.; Lazarides, A. A.; Mirkin, C. A.; Brazis, P. W.; Kannewurf, C. R.; Letsinger, R. L. *Angew. Chem., Int. Ed.* **2000**, *39*, 3845.
(29) Frens, G. *Nat. Phys. Sci.* **1973**, *241*, 20.
(30) Huang, T. C.; Toraya, H.; Blanton, T. N.; Wu, Y. *J. Appl. Crystallogr.* **1993**, *26*, 180.
(31) Glatter, O.; Kratky, O. *Small-Angle X-ray Scattering*; Academic: New York, 1982.
(32) Feigin, L. A.; Svergun, D. I. *Structure Analysis by Small-Angle X-ray and Neutron Scattering*; Plenum Press: New York, 1987.
(33) Composition was done using $^1/_2(1 + \sin(x))$ as a switch function. The relative normalization of the 10 and 240 s profiles was done to have the two profiles overlap for the largest possible extent of scattering vector values.
(34) Equation 1 is exact only in the case of monodisperse systems. For systems with dispersity less than 10%, it provides a useful approximation.
(35) Yanagi, K.; Prive, G. G.; Dickerson, R. E. *J. Mol. Biol.* **1991**, *217*, 201.
(36) Korgel, B. A.; Fitzmaurice, D. *Phys. Rev. B* **1999**, *59*, 14191.
(37) Tkachenko, A. V. *Condens. Matter* **2001**, 1.
(38) Dimon, P.; Sinha, S. K.; Weitz, D. A.; Safinya, C. R.; Smith, G. S.; Varady, W. A.; Lindsay, H. M. *Phys. Rev. Lett.* **1986**, *57*, 595.
(39) Cobbe, S.; Connolly, S.; Ryan, D.; Nagle, L.; Eritja, R.; Fitzmaurice, D. *J. Phys. Chem. B* **2003**, *107*, 470.
(40) Demers, L. M.; Mirkin, C. A.; Mucic, R. C.; Reynolds, R. A.; Letsinger, R. L.; Elghanian, R.; Viswanadham, G. *Anal. Chem.* **2000**, *72*, 5535.
(41) Storhoff, J. J.; Elghanian, R.; Mirkin, C. A.; Letsinger, R. L. *Langmuir* **2002**, *18*, 6666.
(42) Demers, L. M.; Östblom, M.; Jang, N.-H.; Liedberg, B.; Mirkin, C. A. *J. Am. Chem. Soc.* **2002**, *124*, 11248.
(43) For presumably the same reason, particles with poly-adenine spacer maintain their recognition properties for a long period of time (over a year), but particles with poly-thymine spacer tend to lose their recognition properties over time.
(44) Kimura-Suda, H.; Petrovykh, D. Y.; Tarlov, M. J.; Whitman, L. J. *J. Am. Chem. Soc.* **2003**, *125*, 9014.